Conducting Wall Hall Thrusters

IEPC-2013-276

Presented at the 33rd International Electric Propulsion Conference,
The George Washington University • Washington, D.C. • USA
October 6 – 10, 2013

Dan M. Goebel[1], Richard R. Hofer[2], Ioannis G. Mikellides[3], Ira Katz[4], James E. Polk[5] and Brandon Dotson[6]
Jet Propulsion Laboratory, California Institute of Technology, Pasadena, CA 91109

Abstract: A unique configuration of the magnetic field and channel geometry near the wall of Hall thrusters, called "magnetic shielding", has recently demonstrated the ability to significantly reduce the erosion of the boron nitride (BN) walls and extend the life of Hall thrusters by orders of magnitude. The ability of magnetic shielding to minimize interactions between the plasma and the discharge chamber walls in regions where erosion typically occurs has for the first time enabled the replacement of insulating walls with conducting materials *without* loss in Hall thruster performance. It is important to note that this is not a Thruster with Anode Layer (TAL) where the walls are at or near cathode potential, but is a Hall thruster configuration where the walls are near the anode potential. The boron nitride rings in the 6 kW H6 Hall thruster were replaced with graphite that self-biased to near the anode potential during operation. The thruster efficiency remained over 60% (within two percent of the baseline BN configuration) with a small decrease in thrust and increase in Isp typical of magnetically shielded Hall thrusters. The graphite wall temperatures decreased significantly compared to both shielded and unshielded BN configurations, leading to the potential for higher power operation. Eliminating ceramic walls makes it simpler and less expensive to fabricate a thruster to survive launch loads, and the graphite discharge chamber radiates more efficiently which increases the power capability of the thruster compared to conventional Hall thruster designs.

Nomenclature

g	=	acceleration of gravity
Isp	=	specific impulse
$\dot{m}_p$	=	total propellant mass flow rate
T	=	thrust
P_T	=	Total input power
P_d	=	Discharge power
P_{mag}	=	Power into the magnets

I. Introduction

High-power, highly throttleable electric propulsion (EP) enables a significant number of very challenging, high Δv missions by increasing the delivered payload mass and providing rapid transit times relative to other existing propulsion technologies [1,2]. Hall thrusters are prime candidates for many future missions because of their

[1] Senior Research Scientist, Propulsion Group, dan.m.goebel@jpl.nasa.gov
[2] Senior Engineer, Electric Propulsion Group, Jet Propulsion Laboratory, Associate Fellow AIAA
[3] Principal Engineer, Electric Propulsion Group, Jet Propulsion Laboratory, Associate Fellow AIAA
[4] Group Supervisor, Electric Propulsion Group, Jet Propulsion Laboratory, Member AIAA
[5] Principal Engineer, Electric Propulsion Group, Jet Propulsion Laboratory, Associate Fellow AIAA
[6] Graduate Student, California Institute of Technology, Pasadena, CA

higher thrust and lower cost compared to traditional ion thrusters [3,4]. Every Hall thruster fabricated today in the US and Europe has dielectric walls made of either boron nitride (BN) or $BNSiO_2$ [5], or segmented walls that contain both carbon and ceramic material typically in a layered structure [6-8]. This is because these ceramic materials provide:

1) Insulating surfaces so as to not short out the electric field in the thruster acceleration region,
2) Low sputtering yield under ion bombardment to minimize the erosion and extend thruster life,
3) Low secondary electron yield to minimize the electron power loss to the wall.

Hall thrusters that use other wall materials such as higher secondary electron yield ceramics (Al_2O_3, SiC, macor, etc.), or conductors (graphite, carbon velvet, stainless steel, etc.) [9-12] are significantly less efficient and are predicted to have shorter life times and lower throughput capabilities. The poorer performance of thrusters using alternative materials has been largely attributed to the higher secondary yield [13-15] or higher conductivity of these materials compared to the standard BN.

Shortly after the discovery that the erosion of the BN walls in the BPT-4000 Hall thruster designed and developed by Aerojet had essentially stopped after 5,600 hours of operation during life-testing [16], an extensive investigation into the mechanism responsible for this effect was initiated at JPL [17,18]. The erosion of the boron nitride wall in Hall thrusters occurs due to sputtering of the surface by energetic ion bombardment from the plasma in the thruster. The rate of erosion is determined by the energy of the ions, the angle of incidence of the ions, and the flux of ions onto the surface. Numerical simulations performed at JPL with the Hall2De code[19] showed that the BPT-4000 had experienced erosion of the BN walls at rates typical to other Hall thrusters until a certain magnetic field topology was exposed close to the walls near the thruster exit plane that significantly reduced the energy and flux of the ions hitting the wall. This effect has been named "magnetic shielding" [17] and independently verified by modifying another laboratory Hall thruster at JPL to produce the required magnetic topology at the wall [20] to achieve very low erosion rates. Extensive theoretical and experimental efforts have gone into explaining magnetic shielding physics and demonstrating that this effect reduces the erosion of the boron nitride walls by a much as a factor of 1000 [21-23].

Magnetic shielding significantly reduces the plasma contact with the wall in the acceleration region where erosion typically occurs. Experiments on a modified H6 Hall thruster with BN walls at JPL [20] demonstrated that this reduced contact and low wall erosion was achieved with less than 2% change in the thruster efficiency. While the total efficiency was largely unchanged, the thrust was reduced and the Isp increased relative to the baseline performance. The thrust decrease was found to be due to plume divergence angle increases in the magnetically shielded configuration due to the field shape and movement of the plasma downstream by a few millimeters. The Isp increase was found to be due to a larger amount of higher ionized ions in the plume, which increase the ion velocity and therefore the Isp. After testing, the magnetically-shielded H6 BN walls were found to be no longer kept clean from ion sputtering, but were coated with a thin layer of backsputtered carbon from the beam dump. These experiments demonstrated both the reduced erosion of the dielectric surface due to the magnetic field structure, and that the thruster performance was not significantly affected by the presence of a somewhat resistive surface in contact with the plasma due to the thin carbon deposition layer.

To determine if fully conducting walls could be implemented in Hall thrusters, the magnetically-shielded H6 Hall thruster was retrofitted with new walls fabricated of graphite. The H6 thruster is designed with replaceable "rings" near the thruster exit plane where the plasma contacts the walls to provide the ability to measure the erosion rate by removing these rings and measuring the surface profile on precision CMM machines. The selection of graphite as the material for the rings is because it features a low secondary electron yield, a very high emissivity to efficiently radiate any deposited power, and has good strength and a reduced mass compared to stainless steel. Tests at the nominal 6 kW power level of the H6 thruster showed that the fully conductive graphite rings reduced the total thruster efficiency slightly to about 60.5%. The slight difference with magnetic shielding between the graphite wall and the boron nitride wall is not considered significant, and it is probable that further optimization not possible within the limited testing time available to date

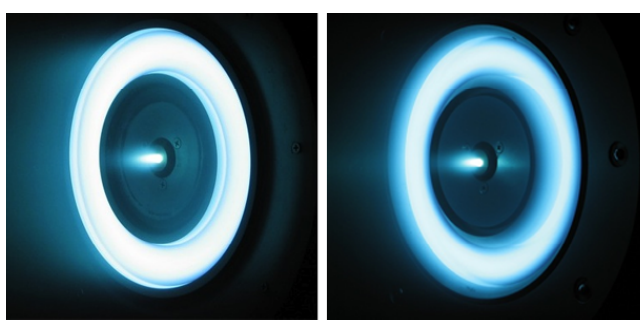

Figure 1. Photograph of the unshielded H6 thruster (left) and magnetically shielded H6 thruster with graphite rings (right) suggesting reduced plasma contact with the walls.

will make up these small differences.

The reduced plasma contact with the wall is visually illustrated by the photos shown in Fig. 1 of the unshielded H6 on the left and the magnetically-shielded graphite-wall H6 on the right; both operating at the same discharge power level of 6 kW. There is a clear visual gap in the magnetically shielded thruster between the wall and the plasma indicative of low excitation and suggesting a detached plasma condition. Detailed probe measurements of this region [18, 21] show low electron temperatures and plasma potentials near the anode potential, which significantly reduce the ion energy striking the wall and reduce the erosion rates. Thermal imaging of the graphite rings, the walls and anode also show a significant decrease in the surface temperature and radiated power at the nominal operating power level. Given this decrease in radiated power as well as the decrease in ring, wall, and anode temperatures observed at even higher operating powers than the nominal 6 kW, it is likely that the use of magnetic shielding techniques and graphite discharge chambers will result in higher power density capabilities in future Hall thrusters of this design.

It is important to recognize that the configuration discussed in this paper is not a so-called "Thruster with Anode Layer "(TAL). A TAL has a similar basic magnetic field configuration as an insulating-wall Hall thruster but with a different electrode design and biasing [5]. While a TAL has a discharge region where the transverse magnetic field lines terminate directly on metallic walls, these walls are usually biased to cathode potential or float close to cathode potential in order to minimize electron energy loss. The significant plasma contact with the metallic walls compresses the acceleration region close to the anode (thus the acronym "anode layer thruster"). The conducting-wall Hall thruster described here has the same geometry as a traditional BN-wall Hall thruster with a deeper channel and near-zero transverse B-field close to the anode compared to a TAL design. This eliminates the anode power loading problems often observed in TAL thrusters, and provides the near-zero wall erosion of a magnetically shielded thruster.

The replacement of traditional ceramic walls with graphite, enabled by the recently discovered magnetic shielding, represents a major advance in Hall thruster technology. This advance greatly simplifies construction of the thruster required to withstand launch vibrations by eliminating large fragile ceramics and their support structures, and will thereby lead to significant reductions in the thruster mass and cost. The new design could also lead to factors of two to three increase in the thruster power density due to the lower power loading on the walls and higher emissivity surfaces, resulting in ultra-compact, very long life Hall thrusters for space missions.

II. Experimental Apparatus

The results presented here are from experiments on the 6-kW H6 Hall thruster [24] that uses an on-axis lanthanum hexaboride (LaB_6) hollow cathode designed specifically for this thruster [25]. The original version of this thruster was a joint development between AFRL, JPL and the University of Michigan [24, 26-29]. The data collected on this thruster at JPL is used to validate plasma simulations [19,23,30] intended to evaluate thrusters being considered for NASA science missions. Details on the experimental configuration and thruster performance can be found in Refs. [21, 31]. The nominal operating parameters and characteristics of the H6 thruster at 6 kW and 300 V in the unshielded BN-wall configuration are found in Table 1.

The experiments were conducted in a 3-m-dia. by 10-m-long vacuum chamber at JPL that was used for the 30,000 hour Extended Life Test of the NSTAR ion thruster [32]. A photograph of the thruster on the thrust stand in the chamber is shown in Fig. 2. The vacuum chamber has a total xenon system pumping speed of approximately 200,000 l/s and produces a background pressure of 1.6×10^{-5} torr at the nominal xenon flow rate of about 21 mg/s at the 6kW operation point. At this background pressure, ingestion from background gases is negligible [33]. The vacuum chamber is lined with graphite panels to reduce the amount of back sputtered material on the thruster and diagnostics. Commercially available power supplies and flow controllers are used to operate the thruster. The propellant flow control system utilized three calibrated xenon mass flow controllers and four 40-V, 19-A laboratory power supplies were used for the

Table 1. Nominal operating conditions for the 6 kW laboratory Hall thruster with the internal cathode.

Parameter	Value
Discharge Voltage (V)	300.0
Discharge Current (A)	20.0
Anode Flow Rate (mg/s)	20.0
Nominal Cathode Flow Rate (mg/s)	1.34
Nominal Cathode to Ground Voltage	-10.8
Nominal Cathode Coupling Voltage	19.6
Ion Current Fractions (plume averaged)	Xe^{+}= 0.75 Xe^{++}= 0.18 Xe^{+++}=0.07
Average Plume Divergence (half angle, defined in Ref. [25])	19°
Nominal Thrust (mN)	392 ±2
Total Efficiency	61-63%
Vacuum Chamber Pressure (torr)	1.6×10^{-5}

inner magnetic coil, outer magnetic coil, internal trim coil, and cathode heater. A 600-V, 2.6-A power supply was used for the cathode keeper. The cathode keeper and heater were turned off once the main thruster discharge was initiated. A data acquisition system was used to monitor the vacuum facility and thruster telemetry. Additional details of the test facility and power electronics can be found in Ref. [21].

The major parameters used to characterize the thruster performance are thrust, specific impulse and total efficiency. The thrust was measured directly by mounting the Hall thruster on the same inverted pendulum thrust stand that was employed in the long duration test (LDT) of the NSTAR ion thruster [34] and modified with stiffer springs and heavier weights to accommodate the higher mass of the Hall thruster. The thrust stand deflection was measured with a linear variable differential transducer (LVDT), and was calibrated by the addition of weights simulating thrust applied to the stand. In order to ensure that long-term drift did not affect the measurements by the thrust stand, calibrations were taken before and after each set of thrust measurements. The absolute uncertainty in the thrust measurement by the calibrated thrust stand is calculated to be 1%.

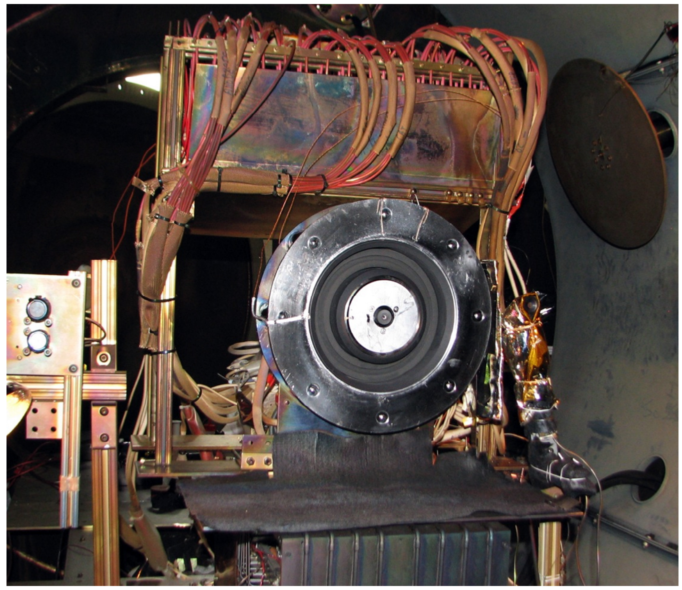

Figure 2. Graphite wall magnetically shielded H6 thruster mounted on the thrust stand in the test chamber at JPL.

The specific impulse (Isp) is given [5] by

$$Isp = \frac{T}{\dot{m}_p g}, \tag{1}$$

where T is the measured thrust, $\dot{m}_p$ is the total propellant mass flow rate and g is the acceleration of gravity = 9.807 m/sec^2. The total efficiency of the thruster is found from

$$\eta_T = \frac{1}{2}\frac{T^2}{\dot{m}_p P_T}, \tag{2}$$

where P_T is the total input power given by

$$P_T = P_d + P_{mag}. \tag{3}$$

In Eq. 3, P_d is the power in the discharge (discharge current times discharge voltage), and P_{mag} is the power in the electromagnets (typically 0.5-1.5% of P_d).

Ring, wall and anode temperatures inside the discharge chamber were remotely measured during these experiments using a FLIR Inframetrics PM 380 Infrared Imaging System. This camera measures the thermal radiation emitted by a surface between wavelengths of 3.4 and 5.0μm with a PtSi/CMOS detector. Each pixel in the detector outputs an 8 bit gray level (GL) value that corresponds to a particular temperature, depending on the emissivity of the radiating surface. Since emissivity is a material property, gray level values are calibrated by heating samples of the same materials found in the thruster with a cathode resistive heater coil and observing the samples mounted next to the thruster. A photograph of the three heated calibration samples (stainless steel (top), graphite (center), and BN (bottom)) after operation with the thruster are shown in Figure 3. Each calibration sample is insulated from the base to avoid conductive losses and is surrounded by radiation shielding as to limit thermal emission from any other surface except the front face. A thermocouple is then inserted from the rear into each sample roughly 0.5mm from the front face in order to provide a physical measurement of the calibration surface temperature. By relating thermocouple and camera gray level values for each of the samples, calibration models are created that allow one to accurately analyze the surface temperatures within the actual thruster.

Since all of the calibration samples have the same surface area and radiating environment, the difference in perceived temperatures for a given camera gray level may be attributed solely to differences in surface emissivity between materials. Therefore, analysis of the calibration results for each of the materials at a fixed gray level enables determination of the effective emissivity for each surface over the measured wavelength range. This is accomplished by comparing the total radiated power of each surface within the given spectrum to that of an ideal black body. Since the effective emissivity of BN is equal to 0.92, there exists some non-physical black body temperature that produces say 8% more total radiated power than the BN surface at a given temperature. In a similar fashion, the total radiated power for the other samples can then be compared to this ideal black body in order to determine the remaining emissivities. Such a calculation yields effective emissivities of 0.70 and 0.96 for the 304 stainless steel and graphite samples respectively, which is well within the published range for these materials.

Figure 3. Stainless steel (top), graphite (center) and boron nitride (bottom) heated samples used for calibration.

Different emissivities among materials could also potentially introduce a large source of error for thermal imaging studies in the form of thin film effects. Throughout several hundred hours of operation, a thin black film is deposited on the surface of the H6 discharge chamber, which is believed to be sputtered, amorphous carbon from the vacuum chamber beam-dump and lining. The presence of such a film makes it difficult to accurately determine wall and ring temperatures given that surface emissivity will change as the film is deposited. In order to investigate this issue, a small strip of the thin black film was removed from the inner and outer walls at different azimuthal locations around the thruster. When viewed using the calibrated thermal imaging camera, these cleaned areas reveal no statistical change in perceived temperature. Despite its true origin, the thin black film and its effects on effective emissivity of the surfaces are therefore considered negligible over the tested operation durations.

III. Experimental Results

The magnetically shielded H6 Hall thruster with graphite walls was tested at power levels of 3 and 6 kW and the performance compared to that measured with the unshielded and shielded H6 thruster with BN walls. The three configurations used for comparison are shown in Fig. 4: unshielded (baseline) with boron nitride rings (left); magnetically shielded with boron nitride rings (middle); and magnetically shielded with carbon rings (right). The baseline and magnetically-shielded H6 configurations with BN walls have each accumulated hundreds of hours of

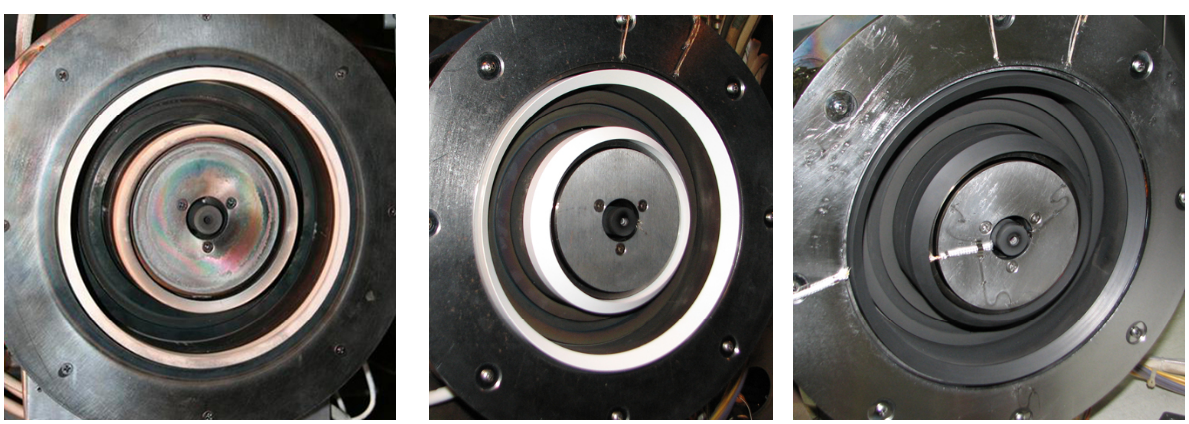

Figure 4. H6 Hall thruster with standard Boron Nitride (BN) rings (left), Magnetically Shielded (MS) BN rings (center), and MS with graphite rings (center).

operating time, and the graphite wall thruster was operated for a total of about 10 hours to ensure that the performance was stable and the thruster was in thermal equilibrium.

A. Thruster Performance

The critical thruster performance data of interest (thrust, Isp and efficiency) were obtained for all three configurations. A comparison of these parameters and the discharge current is shown in Fig. 5 as a function of the inner magnetic field coil current. Plotting the performance results versus this coil current parameter illustrates the variation in performance with magnetic field strength near the exit plane, which is a design parameter in Hall thrusters. The plots clearly show that the magnetically shielded thruster has nearly the same efficiency as the baseline unshielded (within 2%), but the thrust is reduced and the Isp increased relative to the baseline performance. The thrust decrease was found to be due to plume divergence angle increases in the magnetically shielded configuration due to the field shape and movement of the plasma downstream by a few millimeters. The Isp increase was found to be due to a larger amount of higher ionized ions in the plume, which increase the ion velocity and therefore the Isp. Since the channel center-line electron temperature measured in the thruster is not significantly different between shielded and unshielded configurations, it is suggested that the magnetic shielding reduces loss of the tail electron in the Maxwellian electron distribution and these electrons then produce higher charge-state ions observed in the beam.

Replacement of the boron nitride rings with graphite reduced the total thruster efficiency by about another 1%, to a value of about 60.5%, with similar reductions in thrust. The slight difference between the graphite wall and the boron nitride is not considered significant, and it is probable that further optimization will be able to make up these small differences.

It is important to emphasize the significance of these results compared to all previous attempts to change the wall material from BN or BN-based compounds to simple conductors. Figure 6 shows the results from Gascon, et.al, [10] where the thruster behavior with different wall materials was directly compared in the SPT-100 Hall thruster. Utilizing graphite discharge walls reduced the efficiency from the nominal 50% at 300 V of discharge voltage with BN-SiO_2 walls to about 30%. Conducting graphite walls produced the lowest efficiency of any of the materials tested. The use of magnetic shielding to minimize the plasma interaction with the walls removes this dependency and permits high efficiency operation (>60%) to be obtained with conducting walls.

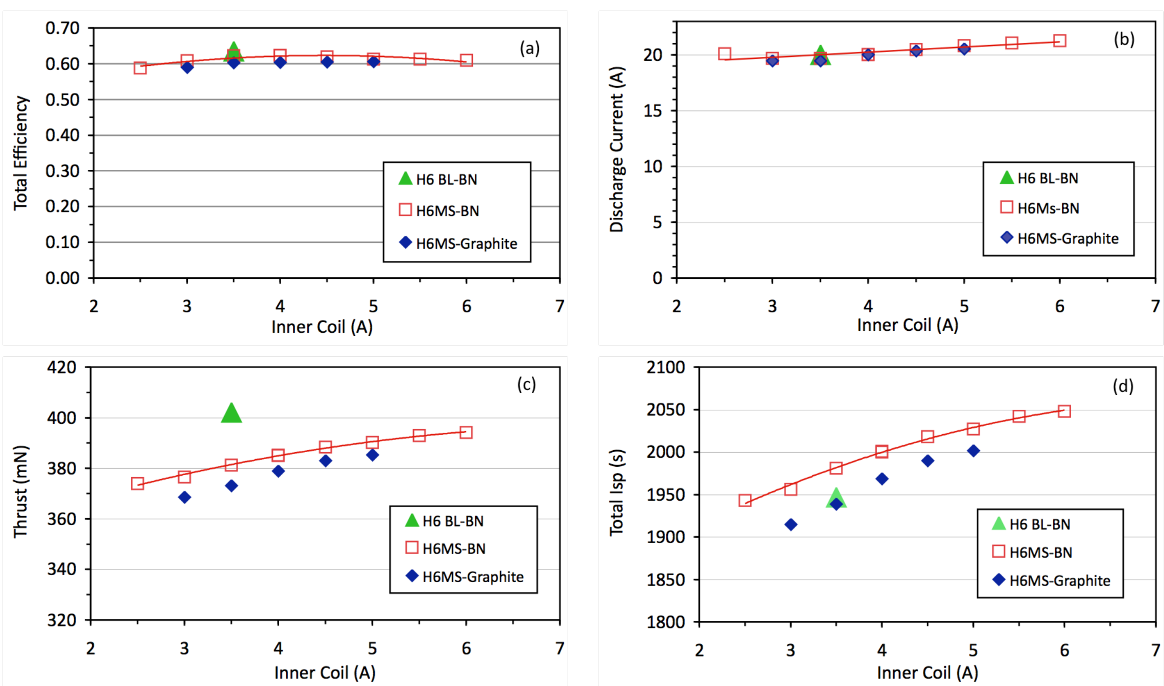

Figure 5. Thruster performance comparison for the three configurations showing, total efficiency (a), discharge current (b), thrust (c) and Isp (d) plotted against inner coil current.

B. Wall Temperatures and Power Level

Calibrated thermal camera measurements of the H6 discharge chamber have been performed for the three thruster configurations over a variety of operating conditions. The observed surfaces include the rings, the discharge chamber wall (between the rings and the anode), and anode in the baseline (BL) and magnetically-shielded (MS) configurations with boron nitride (BN) and graphite rings. Temperatures are given for each configuration with operating powers between 1.5 kW and 6 kW. Moreover, thermocouple measurements of the discharge chamber wall and insert rings have also been used to verify the camera data for the BN-BL and BN-MS experiments.

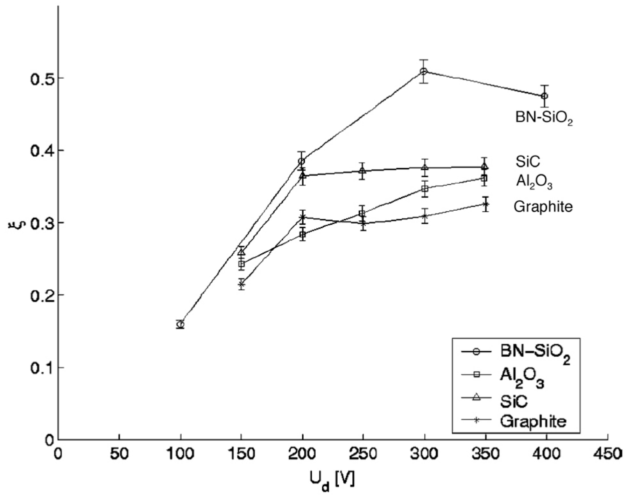

Figure 6. Comparison of the SPT-100 performance with different wall materials showing conducting graphite wall decreased the thruster efficiency to 30% at the nominal 300-V discharge voltage [from Ref. 10].

Graphite and BN ring temperatures for the BL and MS configuration are shown in Fig. 7 as a function of discharge power. The magnitude of the error bars is dominated by the measurement variability from test to test at a given operating condition. For cases with a single test, the uncertainty is estimated conservatively at ±20°C. For a given configuration and power level the inner and outer ring temperatures are the same to within 10-20°C. At 6 kW of thruster power, the steady state ring temperatures in both the BN and graphite MS configurations are roughly 80°C lower than the temperatures in the BL configuration. Such a reduction in ring temperature suggests that altering the magnetic field topology with magnetic shielding successfully decreases plasma bombardment of the BN rings. Additionally, the behavior shown in Fig. 6 suggests that changes in ring temperature are dependent on discharge power; with the use of magnetic shielding and graphite walls having less effect on ring temperatures at lower power densities. Such a trend therefore suggests that applying these thermal management techniques has a high payoff for future high power Hall thruster design.

Discharge chamber wall temperatures are shown in Fig. 8 for the same thruster configurations discussed above. The measurement sites are located approximately in the middle of the discharge chamber wall between the anode and the rings. In this location, the light collected by the thermal camera consists not only of radiation emitted from the surface in view, but also reflected radiation that originated on other discharge chamber components with a line-of-sight view to the wall. The temperatures have not been corrected for this cavity effect and may therefore somewhat overestimate the true temperature, particularly if other components such as the anode are significantly hotter. From these data, there does not appear to be a statistically significant difference in wall temperatures between the MS BN and MS graphite test configurations. However, the MS configuration with BN and graphite rings appears to result in a slight increase in observed temperatures (20-40°C) for the chamber walls, with a larger difference at lower power densities. This behavior suggests that changing the magnetic field topology with magnetic shielding causes a move even distribution of thermal loads inside the discharge chamber and therefore removes the large heat flux to the insert rings as seen in the BL BN configuration.

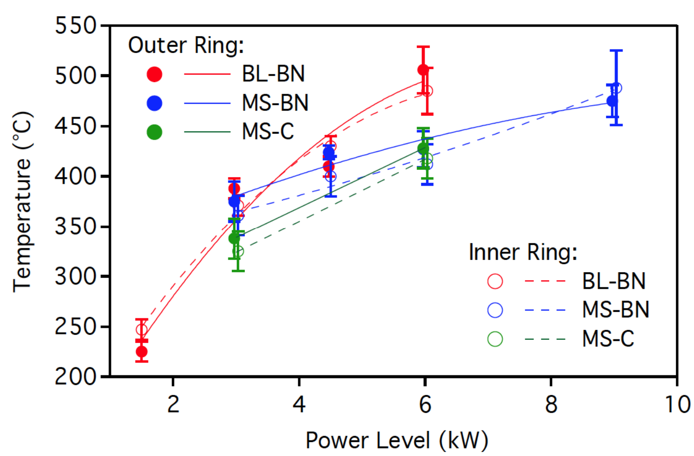

Figure 7. Ring temperatures as a function of discharge power at constant discharge voltage for the three configurations of baseline, magnetically shielded, and graphite walls.

The anode temperatures for the three thruster configurations are plotted in Fig. 9. The anode is made of stainless steel, but is coated with a deposit of carbon from the beam target and possibly boron from the discharge chamber, so it is not clear which emissivity to use in the analysis. Using the stainless steel calibration results in relatively high temperatures, while those obtained with the graphite calibration are close to the temperatures of the other discharge chamber components. These values have also not been corrected for cavity effects, but should accurately reflect qualitative trends with power and thruster configuration. These data exhibit the same behavior as the discharge chamber wall temperatures. The temperatures in the two magnetically shielded configurations are statistically the same and higher than the baseline configuration at lower powers, but all three converge at 6 kW. If the trends continue at higher power levels, the magnetically shielded configuration would have significantly lower temperatures for all discharge chamber components compared to the baseline configuration. In addition, since the walls and rings float at anode potential, it is possible to make them all as a single piece or couple the anode to the walls thermally to provide additional radiation area for the anode heat flux. Graphite has a thermal conductivity twice that of BN [35,36] and a slightly higher emissivity, so it provides an excellent conductive path and serves as an efficient radiator. The flexibility afforded by the conducting wall configuration has the potential to yield a much more robust thermal design.

Using the surface temperature, emissivity, and surface geometry for the insert rings, wall, and anode, the radiated power for each of these components has been estimated and is shown in Table 2. By adding these values together, the total power radiated by the discharge chamber is calculated to be roughly 1055 W, 755 W, and 700W for the BL-BN, MS-BN, and MS-graphite configurations respectively at 6 kW. Thus, replacing the BN insert rings with graphite rings causes a reduction in power losses due to thermal radiation and reduces the radiated power from the rings by more than a factor of 2 compared to the baseline BN configuration. It is posited that this number could be decreased further if the BN discharge chamber walls were also replaced with graphite in the MS configuration. Given this decrease in radiated power as well as the decrease in ring and anode temperatures at higher operating powers, it follows that the use of magnetic shielding techniques and graphite discharge chamber components should be advantageous for future high power Hall thruster designs.

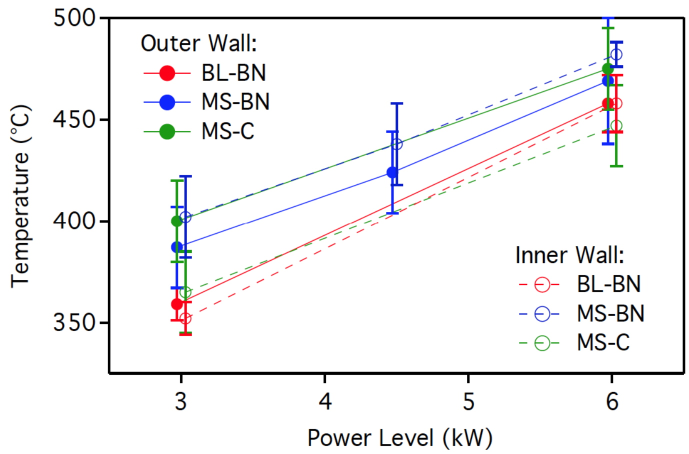

Figure 8. Discharge chamber wall temperatures (upstream of the rings) as a function of discharge power at constant discharge voltage for the three configurations of baseline, magnetically shielded, and graphite walls.

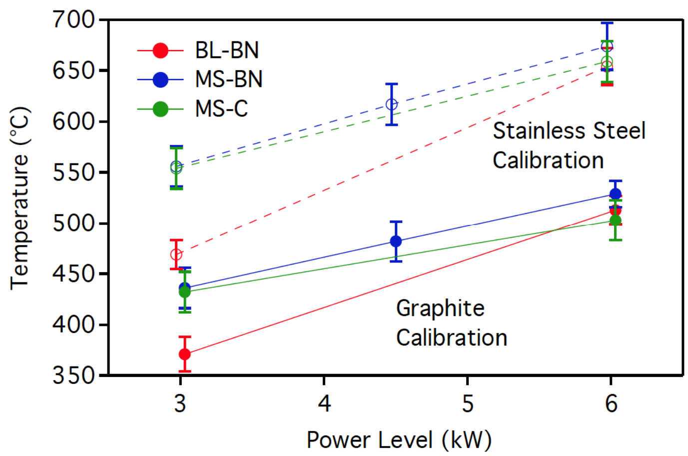

Figure 9. Anode temperatures as a function of discharge power at constant discharge voltage for the three configurations of baseline, magnetically shielded, and graphite walls.

Table 2. Radiated power for each of the discharge chamber components at the nominal 6 kW conditions.

Component	BL BN	MS BN	MS C
Anode	115 W	120 W	110 W
Inner Ring	300 W	150 W	120 W
Outer Ring	310 W	140 W	110 W
Inner Wall	100 W	95 W	100 W
Outer Wall	230 W	250 W	260 W
Total Power	1055 W	755 W	700 W

IV. Discussion

A significant observation made during these tests was that the operation and characteristics of the graphite-wall Hall thruster did not change significantly from the magnetically shielded BN configuration. The optimal magnetic field, the discharge currents and flow rates at the nominal 300 V and 6 kW were unchanged. The discharge was stable and the thruster was turned on and throttled up using the same procedure as the standard BN version. The oscillation levels indicated by the Power Spectral Density (PSD) plots in Fig. 10 were similar to those observed in the magnetic-shielded BN case. The two dominate frequencies with BN walls shown in the figure are at 8.2 kHz and 75 kHz. These same two dominate modes were upshifted slightly to 9.5 kHz and 80 kHz with the graphite walls, and the amplitudes were found to be within about 15% of each other and the BN-walls case.

Another significant observation was the potential of the rings measured during operation. It was observed that at a discharge voltage of 300 V, the floating rings self-biased to 294 ±2 V relative to the cathode. This potential is within about one electron temperature of the plasma potentials measured near the anode and in the magnetically shielded region in front of the rings, which is consistent with the equithermal T_e distribution along the magnetic field lines from the anode region past the rings. Varying the current split between the inner and outer coils in the thruster was used to shift the plasma radially in the channel, and the floating potential of the rings responded to the increased plasma contact and higher electron temperatures during a shift toward the ring by self-biasing further away from the anode potential. Since the majority of the ions are generated in Hall thrusters in the ionization region upstream of the acceleration zone near the thruster exit plane, this self-bias of the graphite walls places them at nearly the same potential as the ion generation region. That means that the ions striking the walls gain little or no energy from the electric field in the Hall thruster that accelerates the beam ions, and so the erosion of the walls is significantly reduced compared to standard unshielded designs. The termination of the magnetic field lines on the iron pole piece on the outside of the thruster

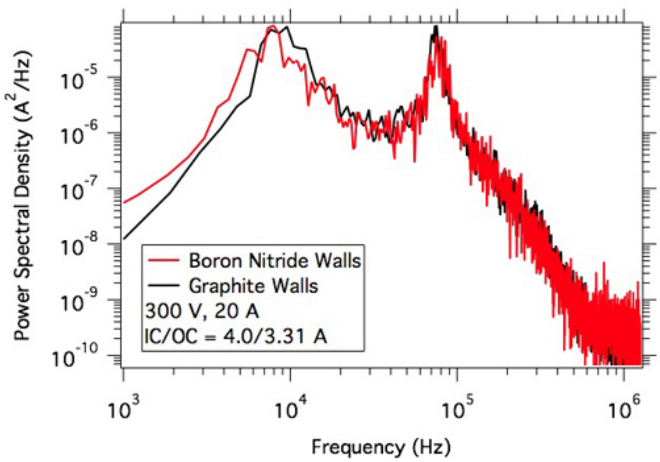

Figure 10. Comparison of the Power Spectral Density (PSD) in the magnetically shielded H6 thruster with BN and graphite walls. The frequency content and behavior is largely the same.

Finally, the higher thermal conductivity and emissivity of graphite suggests that the carbon wall thruster either has significantly more thermal margin than conventional BN wall Hall thrusters, or that it can be configured to run at high power densities without overheating. Since the rings self bias to near the anode potential, it follows that an integral discharge chamber and anode fabricated from a single piece of graphite will tend to conduct the anode power forward in the thruster to be more effectively radiated due to the better view factor to space. It is estimated that the power level might be increased by as much as a factor of two to three, or alternatively a given power thruster could be significantly reduced in size, with this new discharge chamber design.

V. Conclusion

A highly efficient, conducting wall Hall thruster has been fabricated and successfully tested. The ability to replace the ceramic (BN) walls in a traditional Hall thruster with conducting materials such as graphite is enabled by the use of the unique magnetic field tailoring near the wall called "magnetic shielding" that significantly reduces the plasma contact with the walls in regions where erosion typiocally occurs. While the experiments were performed with graphite walls, any material that can withstand the temperatures, such as stainless steel, etc., would work. Tests show that the conducting-wall magnetically-shielded H6 thruster operated at over 60% efficiency at the nominal 300 V and 6 kW power level. The elimination of ceramic walls in Hall thrusters without significant performance penalties opens the design space for lighter, higher-power, lower-cost Hall thrusters, and represents a major advance in thruster technology.

Acknowledgments

The research described in this paper was carried out by the Jet Propulsion Laboratory, California Institute of Technology, under a contract with the National Aeronautics and Space Administration.

References

[1]Brown et al., "Development of High-Power Electric Propulsion Technology for Near-Term and Mid-Term Space Power," JANNAF-1193, 2010.

[2]N. Strange et al., "Solar Electric Propulsion for a Flexible Path of Human Space Exploration," IAC-10.A5.2.4, 2010.

[3]D.Y. Oh, "Evaluation of Solar Electric Propulsion Technologies for Discovery Class Missions", AIAA-2005-4270, 41st Joint Propulsion Conference, Tucson, AZ, July 10-13, 2005.

[4]R.R. Hofer, T.M/. Randolph, D.Y. Oh, J.S. Snyder, "Evaluation of a 4.5 kW Commercial Hall Thruster System for NASA Science Missions", AIAA-2006-4469, 42nd Joint Propulsion Conference, Sacramento, CA, July 9-12, 2006.

[5]D.M. Goebel and I. Katz, *Fundamentals of Electric Propulsion; Ion and Hall Thrusters*, John Wiley and Sons, NJ 2008.

[6]Y. Raitses, D. Staack, A. Dunaevsky, and N. J. Fisch, "Operation of a segmented Hall thruster with low-sputtering carbon-velvet electrodes," *J. Appl. Phys.*, **99** (3), pp. 036103-1–036103-3, Feb. 2006.

[7]Y. Raitses, M. Keidar, D. Staack and N. J. Fisch, "Effects of segmented electrode in Hall current plasma thrusters", J. Appl. Physics, **92** (9), 4906-4911, 2002.

[8]Y. Raitses, D. Staack, and N. J. Fisch, "Controlling the plasma potential distribution in segmented Hall thruster," *IEEE Trans. Plasma Sci.*, **36** (4), pp. 1202–1203, Aug. 2008.

[9]Y. Raitses, J. Ashkenazy, G. Appelbaum, and M. Guelman, "Experimental investigation of the effect of channel material on Hall thruster characteristics," IEPC Paper 97-056, 25th Int. Electric Propulsion Conf., Cleveland, OH, Aug., 1997.

[10]N. Gascon, M. Dudeck, and S. Barral, "Wall material effects in stationary plasma thrusters I: Parametric studies of an SPT-100," *Phys. Plasmas*, **10** (10), pp. 4123–4136, Oct. 2003.

[11]S. Barral, K. Makowski, Z. Peradzynski, N. Gascon, and M. Dudeck, "Wall material effects in stationary plasma thrusters II. Near-wall and in-wall conductivity," *Phys. Plasmas*, **10** (10), pp. 4137–4152, Oct. 2003.

[12]D. Staack, Y. Raitses, and N. J. Fisch, "Control of acceleration region in Hall thrusters," IEPC Paper 03-0273, 28th Int. Electric Propulsion Conf., Toulouse, France, Mar., 2003.

[13]A. Dunaevsky, Y. Raitses, and N. J. Fisch, "Secondary electron emission from dielectric materials of a Hall thruster with segmented electrodes", Physics of Plasmas, **10** (6), 2574-2577, 2003.

[14]Y. Raitses, A. Smirnov, D. Staack, and N. J. Fisch, "Measurements of secondary electron emission effects in Hall thrusters," *Phys. Plasmas*, **13** (1), pp. 014502-1–014502-4, Jan. 2006.

[15]Y. Raitses, et al. "Effect of Secondary Electron Emission on Electron Cross-Field Current in *ExB* Discharges" IEEE T-PS, **39**, pp. 995-1006, (2011).

[16]K.deGrys, A. Mathers, B. Welander, V. Khayms, "Demonstration of 10,400 Hours of Operation on a 4.5 kW Qualification Model Hall Thruster", 46th Joint Propulsion Conference, Nashville, TN, July 25-28, 2010.

[17]I. G. Mikellides, I. Katz, R.R. Hofer, D.M. Goebel, K. deGrys and A. Mathers, "Magnetic Shielding of the Acceleration Channels Walls in a Long-Life Hall Thruster", AIAA-2010-6942, 46th Joint Propulsion Conference and Exhibit, Nashville, TN, July 25-28, 2010.

[18]I.G. Mikellides, I. Katz, R.R. Hofer, D.M. Goebel, and K. deGrys, "Magnetic Shielding of the Channel Walls in a Hall Plasma Accelerator", Physics of Plasmas, **18**, 033501 (2011).

[19]I.G. Mikellides, I. Katz, Numerical simulations of Hall-effect plasma accelerators on a magnetic-field-aligned mesh, Physical Review E, 86 (2012) 046703.

[20]I.G. Mikellides, I. Katz, R.R. Hofer, and D.M. Goebel, "Design of a Laboratory Hall Thruster with Magnetically Shielded Channel Walls, Phase I: Numerical Simulations," AIAA-2011-5809, 47th Joint Propulsion Conference and Exhibit, San Diego, CA, July 31-Aug 3, 2011.

[21]R.R. Hofer, D.M. Goebel, I.G. Mikellides and I. Katz, "Design of a Laboratory Hall Thruster with Magnetically Shielded Channel Walls, Phase II: Experiments", AIAA-2012-3788, 48th AIAA/ASME/SAE/ASEE Joint Propulsion Conference and Exhibit, Atlanta, Georgia, July 30-1, 2012.

[22]I.G. Mikellides, I. Katz, R.R. Hofer, D.M. Goebel, "Design of a Laboratory Hall Thruster with Magnetically Shielded Channel Walls, Phase III: Comparison of Theory with Experiment", AIAA-2012-3789, 48th AIAA/ASME/SAE/ASEE Joint Propulsion Conference and Exhibit, Atlanta, Georgia, July 30-1, 2012

[23]I.G. Mikellides, I. Katz, R.R. Hofer, D.M. Goebel, "Magnetic Shielding of Walls from the Unmagnetized Ion Beam in a Hall Thruster", Appl.Phys.Lett., **102**, 023509 (2013).

[24]J.M. Haas, R.R. Hofer, D.L. Brown, B.M. Reid, and A.D. Gallimore, "Design of the H6 Hall Thruster for High Thrust/Power Investigation," Presented at the 54th JANNAF Propulsion Meeting, Denver, CO, May 14-17, 2007.

[25]D.M. Goebel and R.M. Watkins, "Compact Lanthanum Hexaboride Hollow Cathode", Rev. Sci. Instrum., **81**, 083504, (2010).

[26]D.L. Brown, B.M. Reid, and A.D. Gallimore, R.R. Hofer, J.M. Haas, and C.W. Larson, "Performance Characterization and Design Verification of the H6 Laboratory Model Hall Thruster," Presented at the 54th JANNAF Propulsion Meeting, Denver, CO, May 14-17, 2007.

[27]Brown, D. L., Larson, C. W., Beal, B. E., and Gallimore, A. D., "Methodology and Historical Perspective of a Hall Thruster Efficiency Analysis," Journal of Propulsion and Power 25, 6, 1163-1177 (2009).

[28]Huang, W., Gallimore, A. D., and Hofer, R. R., "Neutral Flow Evolution in a 6-kW Hall Thruster," Journal of Propulsion and Power 27, 3, 553-563 (2011).

[29]Shastry, R., Gallimore, A. D., and Hofer, R. R., "Experimental Characterization of the near-Wall Plasma in a 6-kW Hall Thruster and Comparison to Simulation," AIAA Paper 2011-5589, July 2011.

[30]R.R. Hofer, I. Katz, I. G. Mikellides, D.M. Goebel, K.K. Jameson, R.M. Sullivan, and L.K. Johnson, "Efficacy of Electron Mobility Models in Hybrid-PIC Hall Thruster Simulations", AIAA 2008-4924, 44th AIAA Joint Propulsion Conference, Hartford, CT, July 21 – 23, 2008.

[31]D.M. Goebel, K.K .Jameson and R.R. Hofer, "Hall Thruster Cathode Flow Impacts on Cathode Coupling and Cathode Life", J. of Propulsion and Power, **28**, No.2, pp.355-363, (2012).

[32]A. Sengupta, J.R. Anderson, C. Garner, J.R. Brophy, K. deGroh, B. Banks, and T. Thomas, "Deep Space 1 Flight Space Ion Thruster 30,000 hour Life Test", Journal of Propulsion and Power, **25**, p. 105-117 (2009).

[33]R. R. Hofer, L. K. Johnson, D. M. Goebel, and R.E. Wirz, "Effects of Internally-Mounted Cathodes on Hall Thruster Plume Properties," IEEE Transactions on Plasma Science 36, 5, 2004-2014 (2008).

[34]J.E. Polk, J.R. Anderson, J.R. Brophy, V.K. Rawlin, M.J. Patterson, J. Sovey and J. Hamley, "An Overview of the Results from an 8200 Hour Wear Test of the NSTAR Ion Thruster", AIAA-1999-2446, 35th Joint Propulsion Conference, Los Angeles, CA, June 20-24, 1999.

[35]Manufacturer's data sheet for HP grade Boron Nitride, St. Gobain Ceramics

[36] S. Weisenburger, High Temperatures-High Pressures, Vol.5, p475 (1973).